


Cite this: *RSC Adv.*, 2019, 9, 40811Received 18th September 2019  
Accepted 25th November 2019

DOI: 10.1039/c9ra07535f

rsc.li/rsc-advances

# Au@Co<sub>2</sub>P core/shell nanoparticles as a nano-electrocatalyst for enhancing the oxygen evolution reaction

Xiaofang Zhang, Aixian Shan, Sibin Duan, Haofei Zhao, Rongming Wang \* and Woon-Ming Lau\*

Core/shell nanoparticles (NPs) of Au@Co<sub>2</sub>P, each comprising a Au core with a Co<sub>2</sub>P shell, were prepared, and shown to efficiently catalyze the oxygen evolution reaction (OER). In particular, Au@Co<sub>2</sub>P has a small overpotential of 321 mV at 10 mA cm<sup>-2</sup> in 1 M KOH aqueous solution at room temperature, which is about 95 mV less than pure Co<sub>2</sub>P. More importantly, the Tafel slope of Au@Co<sub>2</sub>P, at 57 mV dec<sup>-1</sup>, is 44 mV dec<sup>-1</sup> lower than that of Co<sub>2</sub>P. Hence, Au@Co<sub>2</sub>P outperforms Co<sub>2</sub>P drastically in practical production when a high current density is required.

## Introduction

Research on electrochemical water-splitting has been intensive, with an objective of resolving the crisis induced by our consumption and depletion of fossil fuels.<sup>1–6</sup> In order to improve the energy efficiency of water-splitting, many electrocatalysts have been designed and applied to catalyze the two half reactions of water electrocatalysis, *i.e.*, the hydrogen evolution reaction (HER) and the oxygen evolution reaction (OER). In this context, the kinetically sluggish OER (4OH<sup>-</sup> → 2H<sub>2</sub>O + 4e<sup>-</sup> + O<sub>2</sub> in base) is a bottle-neck. Therefore, the search for effective catalysts for OER is particularly critical.

Nanoparticles (NPs) with high surface areas are considered to be the preferred form of catalysts. Among them, core/shell NPs composed of hybrid materials at the nanometer scale show remarkable catalytic behavior compared to single-component NPs owing to the cooperative effect of electron transfer between the core and the shell.<sup>7–11</sup> In the design of core/shell NPs as effective catalysts, the shell functions as the catalyst and its composition must meet such functionality. For OER, transition metal oxides and hydroxides have been developed as practical catalysts,<sup>12–15</sup> to replace the expensive bench-marking catalysts derived from oxides of ruthenium and iridium.<sup>16,17</sup> Some of them have indeed demonstrated catalytic activity superior to those ruthenium- and iridium-based catalysts, for a long operation-period at extremely high current densities.<sup>18</sup> Recently, transition metal phosphides, particularly those of Ni and Co, have emerged as active electrocatalysts for water

splitting.<sup>19–23</sup> To extend this trend with the design philosophy of core/shell NPs for enhancing the catalytic efficiency of the bare shell materials, researchers have explored mixing transition-metal-based catalysts with carbon,<sup>24–26</sup> and with other transition metal (including noble metal).<sup>27,28</sup> Among these trials, the incorporation of gold in catalysts derived from transition-metal-oxides show very promising results.<sup>29–32</sup> For example, Au@NiO<sub>x</sub>, Au@CoO<sub>x</sub>, and Au@CoFeO<sub>x</sub> core/shell NPs all exhibit enhanced OER activity in reference to the corresponding oxides without Au.<sup>33</sup> Similarly, Au@Ni<sub>12</sub>P<sub>5</sub> NPs all show superior OER activity in reference to Ni<sub>12</sub>P<sub>5</sub> NPs.<sup>34</sup> These recent progresses encourage further search for efficient and stable core/shell NPs as OER catalysts.

Herein, we have prepared core/shell NPs each comprising an Au core and a Co<sub>2</sub>P shell, and examined their OER electrocatalytic performance. The mechanism of the enhancement effect of the Au core over the catalytic performance of Co<sub>2</sub>P, in the framework of electron transfer from the Co<sub>2</sub>P shell to the Au core, is elaborated.

## Experimental section

### Reagents and instrument

Gold(III) chloride hydrate [HAuCl<sub>4</sub>·4H<sub>2</sub>O, 99%], cobalt(II) acetylacetonate [Co(acac)<sub>2</sub>, 97%], and triphenylphosphine (TPP, 97%) were purchased from Sigma-Aldrich. Anhydrous ruthenium(IV) oxide [RuO<sub>2</sub>, 99.9%] was purchased from Alfa Aesar. Oleylamine [OAm, 70%] and Co<sub>2</sub>P (98%) were purchased from Aladdin. All chemicals were used without further purification.

The crystal structures, morphologies, and chemical compositions of the prepared Au@Co<sub>2</sub>P NPs were studied using X-ray diffraction (XRD, X'Pert Pro MPD system, Cu-Kα) and transmission electron microscopy (TEM, Titan ETEM G2 with a 300 kV field emission gun). The elemental composition

Beijing Advanced Innovation Center for Materials Genome Engineering, Center for Green Innovation, Beijing Key Laboratory for Magneto-Photoelectrical Composite and Interface Science, School of Mathematics and Physics, University of Science and Technology Beijing, Beijing 100083, China. E-mail: rmwang@ustb.edu.cn; leolau@ustb.edu.cn



distributions were measured by the TEM with energy dispersive X-ray spectroscopy (EDS, Oxford 80T). X-ray photoelectron spectroscopy (XPS) was performed with a PHI 5000 VersaProbe spectrometer.

### Synthesis of Au@Co<sub>2</sub>P NPs

The Au@Co<sub>2</sub>P core/shell NPs were synthesized *via* a method based on our previous work.<sup>34,35</sup> Firstly, Co(acac)<sub>3</sub> (0.5 g) and oleylamine (OAm, 10 mL) were added into a three-necked flask, and mixed at 100 °C for 60 min. Secondly, the prepared solution of HAuCl<sub>4</sub>·4H<sub>2</sub>O (10 mg mL<sup>-1</sup> in toluene) was maintained at 100 °C for 120 min under the protection of argon (40 mL min<sup>-1</sup>). Thirdly, triphenylphosphine (TPP) (1.0 g) was added into the above solution and the mixture was stirred for 30 min. Then the solution was heated to 300 °C for 120 min. Finally, the prepared Au@Co<sub>2</sub>P core/shell NPs were collected, cleaned, and stored as a colloid in toluene.

### Electrode preparation

The as-synthesized NPs were firstly dispersed in a Nafion solution (ethanol/H<sub>2</sub>O/Nafion = 50 : 199 : 1) to a concentration of 2 mg mL<sup>-1</sup>, as a catalyst ink. Then 20 µL of the catalyst ink was drop-casted onto a rotating disc electrode (RDE) with a diameter of 5 mm (the carbon-supported catalyst loading mass was 0.20 mg cm<sup>-2</sup>).

### Electrochemical measurements

All the electrochemical measurements were conducted in a typical three-electrode setup with an Hg/HgO (in 1 M KOH solution) electrode as the reference electrode, and a Pt foil electrode (1 cm<sup>2</sup>) as the counter electrode. The potentials measured were then calibrated against the reversible hydrogen electrode (RHE). Linear sweep voltammetry (0.05 to -0.8 V) with a scan rate of 2 mV s<sup>-1</sup> in 1 M KOH was performed and the data were used to deduce the catalyst-performance for OER.

## Results and discussion

### Fabrication and growth process of Au@Co<sub>2</sub>P NPs

The mechanism in synthesizing the Au@Co<sub>2</sub>P NPs in this work is basically a seed-mediated growth, and the reaction processes are illustrated in Fig. 1a. Briefly, Au NPs are firstly formed by reducing HAuCl<sub>4</sub> in an OAm solution to yield Au-nuclei and by using TPP as a surfactant to curb any excessive growth of these Au-nuclei (Fig. 1b). Subsequently, Co ions are reduced and metallic Co is deposited onto the Au-nuclei for the formation of Au@Co NPs (Fig. 1c). The gradual phosphating of Au@Co NPs to yield Au@Co<sub>2</sub>P NPs is traced by the changes in the selected area electron diffraction (SAED) patterns and the lattice images, and the results are shown in Fig. 1c and d. In addition, the high resolution transmission electron microscopy (HR-TEM) images at different growth-stages also show that spherical Au NPs are firstly formed with an average diameter of 8.2 ± 2.5 nm (Fig. 1b), with the subsequently formation of Au@Co and Au@Co<sub>2</sub>P NPs (Fig. 1c and d). The size range of Au@Co<sub>2</sub>P NPs spans from 15–25 nm.

### Morphology and composition characterization

Further, High-Angle Annular Dark Field (HAADF) TEM images reveal that the prepared Au@Co<sub>2</sub>P NPs are near spherical in morphology (Fig. 2a). Furthermore, the distribution of atomic components in the core and the shell can be well revealed by the TEM image. The Au core has a larger atomic number than Co<sub>2</sub>P shell, hence, appears in a dark contrast in this image. As shown in Fig. 2b, the HR-TEM image exhibits that the Au@Co<sub>2</sub>P NPs are well-crystallized. The interplanar *d*-spacing of about 0.22 nm of Au reveals the presence of the (111) lattice fringes of metallic Au in the core. On the other hand, the interplanar *d*-spacing of about 0.18 nm confirms the presence of the (130) lattice fringes of Co<sub>2</sub>P. The lattice spacing of Au in the core is slightly less than its common values of 0.23–0.24 nm, indicating that the Au core is strained and suppressed by the Co<sub>2</sub>P shell. The HRTEM also suggests the presence of an amorphous overlayer at the outer surface of the Co<sub>2</sub>P shell, with a thickness of around 1–2 nm. Naturally, Co<sub>2</sub>P is expected to be oxidized and passivated when it is exposed to oxygen or air. Hence, this amorphous overlayer is likely formed due to the oxidation of Co<sub>2</sub>P. Such oxidation is later elaborated with the following composition analyses of Au@Co<sub>2</sub>P NPs.

The composition of Au@Co<sub>2</sub>P is first identified with EDS (Fig. 2c–g). The stoichiometry of Co<sub>2</sub>P in the shell and the presence of pure Au in the core are confirmed. X-ray diffraction (XRD) patterns of the prepared Au@Co<sub>2</sub>P NPs are shown in Fig. 3a. The four observable peaks at 38.2°, 44.4°, 64.6°, and 77.5° are respectively assigned to the Au (111), (200), (220) and (311) lattice planes (PDF#04-0784). The peaks at 40.7°, 44.5°, 48.81°, 52.15°, and 56.27° are respectively assigned to the Co<sub>2</sub>P (121), (130), (031), (131), (320) lattice planes (PDF#32-306).<sup>36,37</sup>

Additional compositional and electronic information are revealed by XPS. All high-resolution spectra are calibrated against the C 1s line at 284.8 eV arising from the presence of adventitious C. Briefly, the presence of Co, P and Au are confirmed by XPS. Details in chemical states and electron-transfer are revealed by those high resolution spectra included in Fig. 3b–d. First, the P 2p spectrum clearly displays two spectral groups each of which can be fitted to a pair of P 2p<sub>3/2</sub> and P 2p<sub>1/2</sub> (2 : 1 ratio in relative intensity and spin-orbit splitting of 0.86 eV) (Fig. 3b). The spectral group of P 2p<sub>3/2</sub> at 128.4 eV is attributed to the presence of Co<sub>2</sub>P, and that at 131.9 eV to phosphate derived from the surface oxidation and passivation of Co<sub>2</sub>P.<sup>38–42</sup> By the intensity ratio of phosphate/phosphide and with the standard XPS overlayer-measurement method applicable to the present situation: thickness = 3 nm × ln (phosphate/phosphide + 1), we estimate that the phosphate overlayer thickness is ~2 nm. Although this method merely gives a rough estimate due to the particulate-nature of the XPS sample, the presence of a phosphate overlayer is evident and its thickness of ~2 nm is consistent to the TEM result in Fig. 2b. Second, the high resolution Co 2p<sub>3/2</sub> spectrum shows the presence of Co<sub>2</sub>P at 777.5 eV (Fig. 3c)<sup>38</sup> and Co-phosphate at 781.6 eV.<sup>29</sup> The surface oxidation of Co<sub>2</sub>P due to air exposure and due to OER may also lead to the formation of various Co-oxides which have XPS



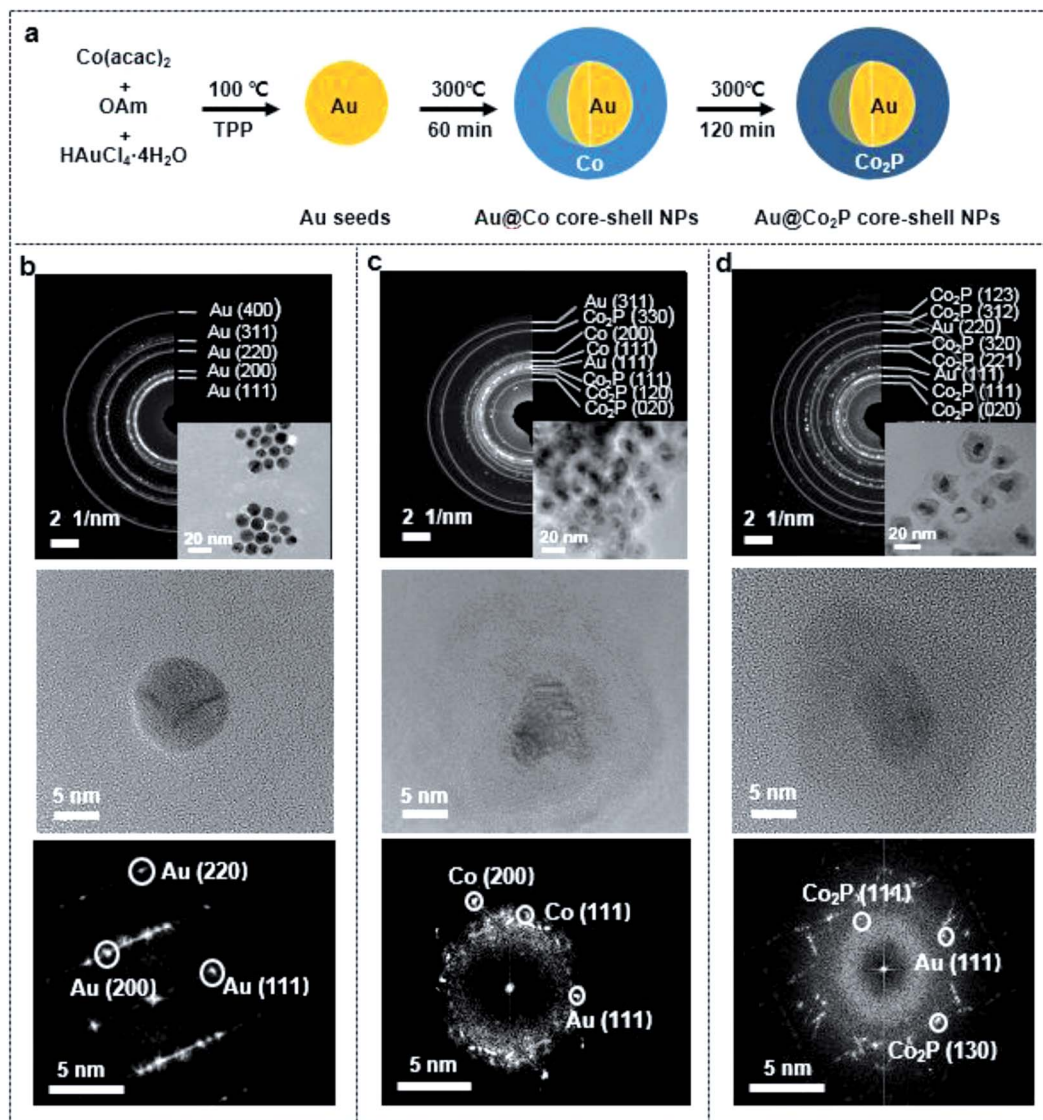


Fig. 1 (a) Schematic fabrication process of the Au@Co<sub>2</sub>P core-shell NPs via seed-mediated growth. (b–d) The selected area electron diffraction (SAED) patterns, HR-TEM images and FFT images of the reaction intermediate/product in the growth of Au@Co<sub>2</sub>P NPs: (b) core of Au NPs; (c) Co-shell enclosing the Au core; (d) Au@Co<sub>2</sub>P. The insets in SAED of (b)–(d) are the corresponding TEM images.

binding energies (BE) around 781.6 eV. Hence, the scientific identity of Co-phosphate in the present work is not exact and is likely a composite of Co-phosphate and various forms of Co-oxides/hydroxides. The broad peak at about 785 eV is commonly known as XPS satellite in association with Co 2p<sub>3/2</sub>. In short, both the P 2p and Co 2p<sub>3/2</sub> XPS results clarify that the Co<sub>2</sub>P of Au@Co<sub>2</sub>P is naturally oxidized to yield an intriguing structure comprising an Au core, a Co<sub>2</sub>P inner shell, and a Co-phosphate outer shell. Obviously, OER takes place on the outer shell of Co-phosphate, hence, Co-phosphate is the actual OER catalyst. While Co<sub>2</sub>P is metallic, Co-phosphate and Co-oxides/hydroxides are semiconducting. On a semiconductor, OER can only proceed with an external voltage-bias such that the OER electrochemical potential is close to the valence band maximum (VMB) of the semiconductor for electrons releasing from OER to drain to the empty electron states at VBM.

The following XPS spectra give some hints on how this mechanism works. First, the Au 4f<sub>7/2</sub> and Au 4f<sub>5/2</sub> spectra in Fig. 3d reveal their respective BE at 83.7 eV and 87.5 eV. These are slightly smaller than those for pure gold (4f<sub>7/2</sub>: 84 eV, 4f<sub>5/2</sub>: 87.8 eV). Hence, the core of Au in Au 4f<sub>7/2</sub> and Au 4f<sub>5/2</sub> is slightly more electron-rich than pure-gold. Second, the P 2p and Co 2p<sub>3/2</sub> of pure Co<sub>2</sub>P (in NPs) are also quite different from those of Au@Co<sub>2</sub>P. The differences are: (a) the phosphate/phosphide ratio is much higher in Co<sub>2</sub>P than that in Au@Co<sub>2</sub>P; hence, the presence of electron-withdrawing gold as the core constituent in Au@Co<sub>2</sub>P retards the surface oxidation of Co<sub>2</sub>P. We speculate that this passivation effect may raise the stability of Au@Co<sub>2</sub>P in OER. (b) All peaks in Co<sub>2</sub>P are up-shifted in XPS BE by about 0.7 eV in reference to those in Au@Co<sub>2</sub>P. Since in the present analysis case, XPS spectra data are collected with a semiconductor (phosphate or oxide/hydroxide) connecting to





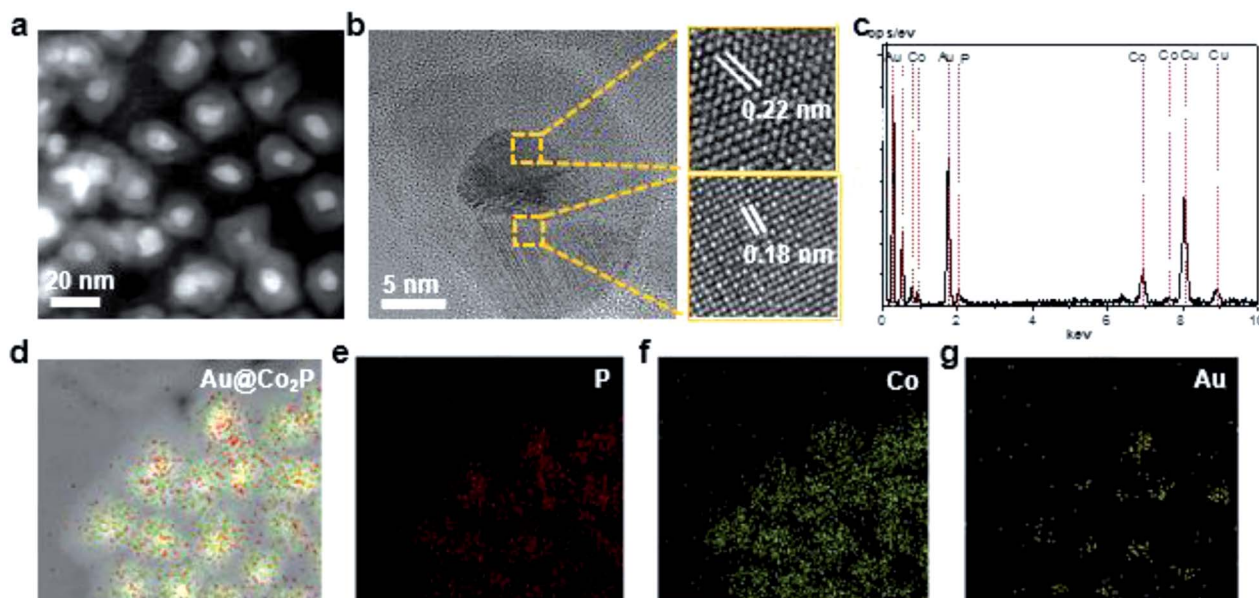


Fig. 2 (a) HAADF TEM images of the prepared Au@Co<sub>2</sub>P core/shell NPs. (b) HR-TEM image of well-crystallized Au@Co<sub>2</sub>P NPs, revealing the lattice fringes of core/shell NPs. (c) EDS spectrum of Au@Co<sub>2</sub>P NPs, confirming the Co<sub>2</sub>P stoichiometry. (d–g) EDS elemental mapping images of Au@Co<sub>2</sub>P NPs.

the XPS spectrometer and with other sample-constituents (phosphide and gold) inside the semiconductor, all spectral peak positions are affected by the Fermi level position of the semiconductor. Take a simple example of a semiconductor with

a bandgap energy of 1 eV, the Fermi level of an n-type semiconductor is located near the conduction band minimum and that of a p-type semiconductor is near the VBM, with a difference of 1 eV. Hence, the XPS peaks of the p-type semiconductor

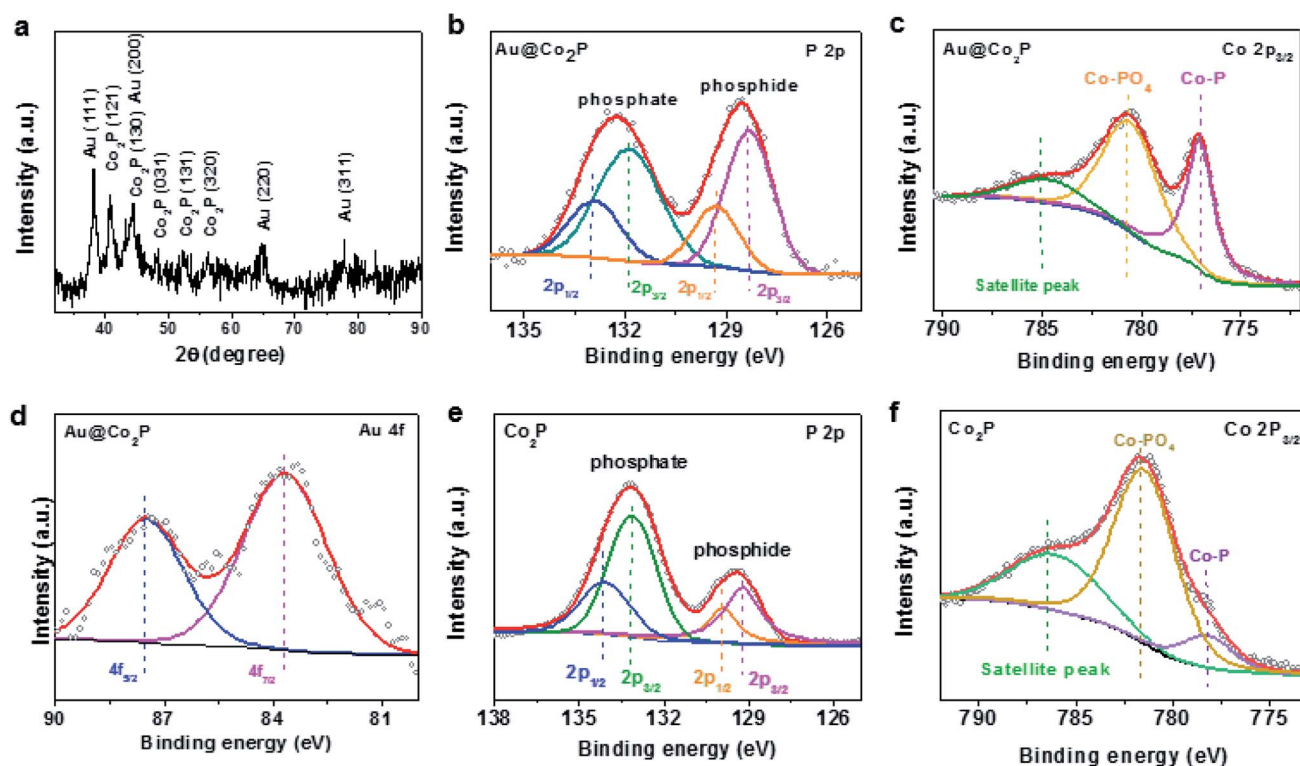


Fig. 3 (a) XRD patterns of the prepared Au@Co<sub>2</sub>P NPs. (b) P 2p, (c) Co 2p<sub>3/2</sub>, and (d) Au 4f XPS spectra of Au@Co<sub>2</sub>P core/shell NPs, respectively. (e) P 2p, (f) Co 2p<sub>3/2</sub> XPS spectra of Co<sub>2</sub>P, respectively.



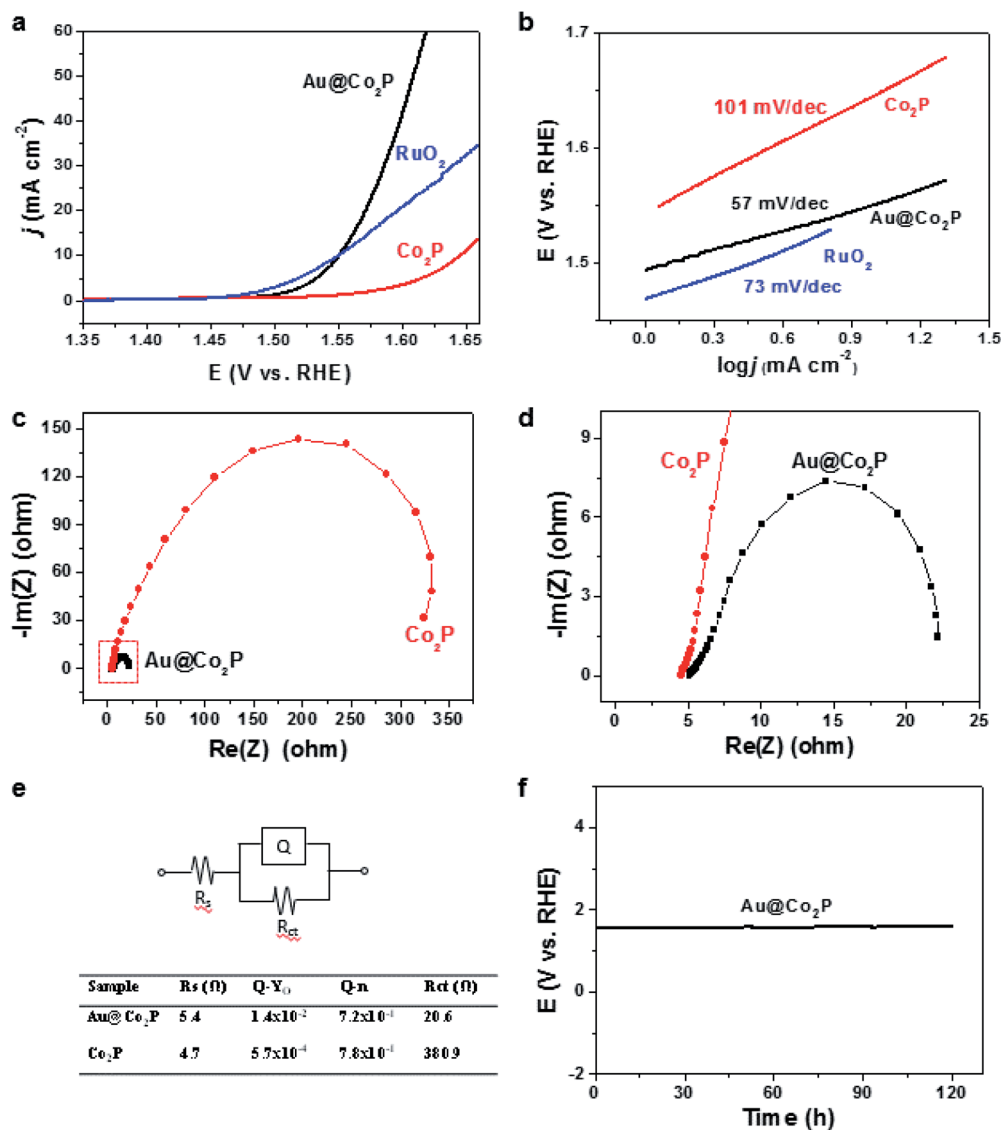


Fig. 4 (a) Polarization curves of Au@Co<sub>2</sub>P core/shell NPs, Co<sub>2</sub>P and RuO<sub>2</sub>. (b) Tafel plots of Au@Co<sub>2</sub>P core/shell NPs, Co<sub>2</sub>P and RuO<sub>2</sub>. (c) Nyquist plots of Au@Co<sub>2</sub>P and Co<sub>2</sub>P. (d) The enlarged view of the dash line area of the plot (c). (e) The equivalent circuit and the corresponding data. (f) Stability of Au@Co<sub>2</sub>P (chronopotentiometry curve).

are expected to down-shift in BE by about 1 eV in reference to those of the n-type semiconductor. With this simple example, we hypothesize that the Fermi level of the Co-phosphate semiconductor of Au@Co<sub>2</sub>P is closer to the VBM of Co-phosphate by 0.7 eV than that of Co<sub>2</sub>P. Since OER is facilitated by electron-drainage to the VBM of Co-phosphate, the OER overpotential of Au@Co<sub>2</sub>P must be significantly lower than that of Co<sub>2</sub>P. The Fermi level movement from Co<sub>2</sub>P to Au@Co<sub>2</sub>P, with a movement direction towards the VBM of the phosphate-semiconductor is driven by the incorporation of gold as a core constituent in Au@Co<sub>2</sub>P. In our hypothesis, gold has a work-function higher than those of Co<sub>2</sub>P and Co-phosphate, and this induces the observed Fermi level movement in favour of OER catalysis.

### Electrochemical properties of Au@Co<sub>2</sub>P NPs

The OER activities of the Au@Co<sub>2</sub>P NPs are best expressed by the polarization curves in Fig. 4a. The results show that Au@Co<sub>2</sub>P has an overpotential of 321 mV at a current density of 10 mA cm<sup>-2</sup>. This overpotential is about 95 mV less than that of pure Co<sub>2</sub>P (416 mV) and nearly the same as that of RuO<sub>2</sub> (320 mV). At a potential of 1.60 V vs. RHE, Au@Co<sub>2</sub>P and Co<sub>2</sub>P reach current densities of 41.08 mA cm<sup>-2</sup> and 3.47 mA cm<sup>-2</sup>, respectively. The superiority of Au@Co<sub>2</sub>P to Co<sub>2</sub>P is obvious.

As shown in Fig. 4b, Au@Co<sub>2</sub>P and Co<sub>2</sub>P display small Tafel slopes, which are about 57 and 101 mV dec<sup>-1</sup>, respectively. Hence, Au@Co<sub>2</sub>P outperforms Co<sub>2</sub>P, particularly in conditions when high current densities are demanded. The Tafel slope of Au@Co<sub>2</sub>P is also smaller than that of RuO<sub>2</sub> (73 mV dec<sup>-1</sup>).



Nyquist plots of Au@Co<sub>2</sub>P and Co<sub>2</sub>P (Fig. 4c–e) indicate that the charge-transfer resistance of Au@Co<sub>2</sub>P (20.6  $\Omega$ ) is much smaller than Co<sub>2</sub>P (380.9  $\Omega$ ). The long term stability test for the OER of Au@Co<sub>2</sub>P in 1 M KOH at 10 mA cm<sup>−2</sup> confirms, as shown in Fig. 4f, that the Au@Co<sub>2</sub>P catalytic effect is stable in the testing duration of 122 hours.

Finally, the critical presence of phosphate after the long stability test is confirmed by XPS, as shown in Fig. 5. For both Au@Co<sub>2</sub>P and Co<sub>2</sub>P, XPS analyses give evidence of the presence of phosphate and the growth of phosphate in the expense of phosphide oxidation (at least in the nanometer-thickness scale of XPS) after a prolonged OER of 122 hours. A comparison of the XPS atomic compositional measurements, expressed in Co, P, and O, before and after such a prolonged trial of OER shows that although the presence of phosphate is evident after the prolonged trial, the P/Co and P/O concentration-ratios decrease greatly after the trial. Hence, Co-phosphide is effectively converted to Co-phosphate and various forms of Co-oxides/hydroxides, and the oxides/hydroxides become the dominant oxidation products after a prolonged trial of OER. Dynamic evolution like this has also been found and reported.<sup>43</sup> In addition, the conversion of Co-phosphate to Co-oxides/hydroxides in alkaline OER conditions has also been previously reported.<sup>13,20,23,27,28,38,42</sup> However, a comparison of the published works on OER performance of Co-phosphate and Co-oxides/hydroxides reveals no large differences in OER overpotential among them.<sup>12,27,33,38</sup> As such, this comparative analysis also explains the seemingly-contradicting observations in this work that although the presence of Co phosphate in Au@Co<sub>2</sub>P in the prolonged OER trial is dynamically overtaken by the presence of Co oxides/hydroxides, the catalytic performance of such nominal Au@Co<sub>2</sub>P remains virtually unchanged and stable as shown in Fig. 4f. In short, this examination confirms that phosphide is merely a precursor for the formation of the real OER catalyst of Co-phosphate and/or Co-oxides/hydroxides. Further studies of the exact roles of Co-phosphate, Co-oxides, Co-hydroxides, and the composites and derivatives of these species in OER are critical.

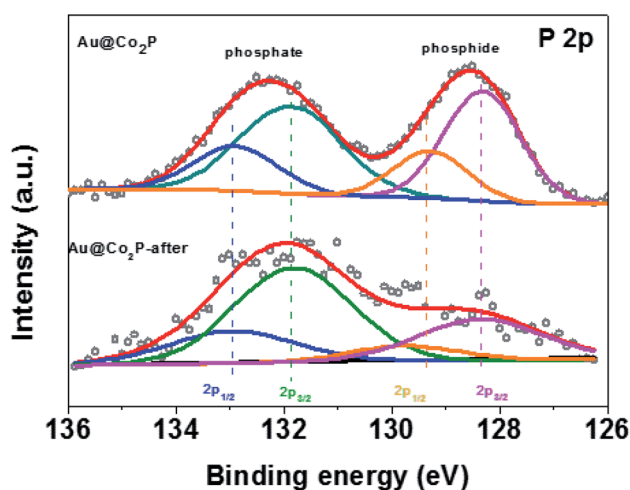


Fig. 5 P 2p of Au@Co<sub>2</sub>P after OER tests in comparison with those before OER tests.

## Conclusions

Core-shell Au@Co<sub>2</sub>P NPs are synthesized *via* a wet chemical method and their catalytic OER performance is examined. A relatively small OER overpotential of 321 mV at 10 mA cm<sup>−2</sup>, with a long stability of over 122 hours, is evident. The Tafel slope of 57 mV dec<sup>−1</sup> is smaller than that of Ru-oxide. In comparison, Co<sub>2</sub>P NPs with no core-Au show an OER overpotential of 416 mV and Tafel slope of 101 mV dec<sup>−1</sup>. A set of comprehensive analyses reveals that the natural surface-oxidation processes of Co<sub>2</sub>P to form Co-phosphate and Co-oxides/hydroxides are critical. As such, the phosphide (Co<sub>2</sub>P) is merely a precursor. The real OER catalyst is derived from the oxidation of Co<sub>2</sub>P and is a semiconductor. In accord to the basic science of a semiconducting catalyst in electrochemistry, the Fermi level position of the semiconducting catalyst is affected by the core-Au of the semiconducting catalyst, and this affects the OER activity.

## Conflicts of interest

There are no conflicts to declare.

## Acknowledgements

This work was supported by the National Natural Science Foundation of China no. 21601013, no. 11674023, 111 Project no. B170003 and the Fundamental Research Funds for the Central Universities no. FRF-TP-17-072A1.

## References

- W. Leitner, J. Klankermayer, S. Pischinger, H. Pitsch and K. Kohse-Hoinghaus, Advanced biofuels and beyond: chemistry solutions for propulsion and production, *Angew. Chem., Int. Ed.*, 2017, **56**, 5412.
- S. E. Habas, H. A. Platt, M. F. van Hest and D. S. Ginley, Low-cost inorganic solar cells: from ink to printed device, *Chem. Rev.*, 2010, **110**, 6571.
- L. Lu, T. Zheng, Q. Wu, A. M. Schneider, D. Zhao and L. Yu, Recent advances in bulk heterojunction polymer solar cells, *Chem. Rev.*, 2015, **115**, 12666.
- G. Tan, L. D. Zhao and M. G. Kanatzidis, Rationally designing high-performance bulk thermoelectric materials, *Chem. Rev.*, 2016, **116**, 12123.
- J. R. McKone, S. C. Marinescu, B. S. Brunschwig, J. R. Winkler and H. B. Gray, Earth-abundant hydrogen evolution electrocatalysts, *Chem. Sci.*, 2014, **5**, 865.
- M. S. Dresselhaus and I. L. Thomas, Alternative energy technologies, *Nature*, 2001, **414**, 332.
- C. J. Zhong and M. M. Maye, Core-shell assembled nanoparticles as catalysts, *Adv. Mater.*, 2001, **13**, 1507.
- T. Hirakawa and P. V. Kamat, Charge separation and catalytic activity of Ag@TiO<sub>2</sub> core-shell composite clusters under UV-irradiation, *J. Am. Chem. Soc.*, 2005, **127**, 3928.
- K. Maeda, K. Teramura, D. L. Lu, N. Saito, Y. Inoue and K. Domen, Noble-metal/Cr<sub>2</sub>O<sub>3</sub> core/shell nanoparticles as



- a cocatalyst for photocatalytic overall water splitting, *Angew. Chem., Int. Ed.*, 2006, **45**, 7806.
- 10 V. Mazumder, M. F. Chi, K. L. More and S. H. Sun, Core/shell Pd/FePt nanoparticles as an active and durable catalyst for the oxygen reduction reaction, *J. Am. Chem. Soc.*, 2010, **132**, 7848.
  - 11 P. Strasser, S. Koh, T. Anniyev, J. Greeley, K. More, C. F. Yu, Z. C. Liu, S. Kaya, D. Nordlund, H. Ogasawara, M. F. Toney and A. Nilsson, Lattice-strain control of the activity in dealloyed core-shell fuel cell catalysts, *Nat. Chem.*, 2010, **2**, 454.
  - 12 Z. Zhuang, W. Sheng and Y. Yan, Synthesis of monodisperse Au@Co<sub>3</sub>O<sub>4</sub> core-shell nanocrystals and their enhanced catalytic activity for oxygen evolution reaction, *Adv. Mater.*, 2014, **26**, 3950.
  - 13 Z. Wu, Q. Gan, X. Li, Y. Zhong and H. Wang, Elucidating surface restructuring-induced catalytic reactivity of cobalt phosphide nanoparticles under electrochemical conditions, *J. Phys. Chem. C*, 2018, **122**, 2848.
  - 14 J. Xin, H. Tan, Z. Liu, L. Zhao, J. Xie, Y. Sang, W. Zhou, A. Wang, H. Liu and J. Wang, Facile synthesis of hierarchical porous Ni<sub>x</sub>Co<sub>1-x</sub>SeO<sub>3</sub> networks with controllable composition as a new and efficient water oxidation catalyst, *Nanoscale*, 2019, **11**, 3268.
  - 15 F. Yu, L. Yu, I. Mishra, Y. Yu, Z. Ren and H. Zhou, Recent developments in earth-abundant and non-noble electrocatalysts for water electrolysis, *Materials Today Physics*, 2018, **7**, 121.
  - 16 F. I. Mattos-Costa, P. de Lima-Neto, S. A. S. Machado and L. A. Avaca, Characterisation of surfaces modified by sol-gel derived Ru<sub>x</sub>Ir<sub>1-x</sub>O<sub>2</sub> coatings for oxygen evolution in acid medium, *Electrochim. Acta*, 1998, **44**, 1515.
  - 17 H. Over, Surface chemistry of ruthenium dioxide in heterogeneous catalysis and electrocatalysis: from fundamental to applied research, *Chem. Rev.*, 2012, **112**, 3356.
  - 18 H. Zhou, F. Yu, Q. Zhu, J. Sun, F. Qin, L. Yu, J. Bao, Y. Yu, S. Chen and Z. Ren, Water splitting by electrolysis at high current densities under 1.6 volts, *Energy Environ. Sci.*, 2018, **11**, 2858.
  - 19 Y. Shi and B. Zhang, Recent advances in transition metal phosphide nanomaterials: synthesis and applications in hydrogen evolution reaction, *Chem. Soc. Rev.*, 2016, **45**, 1529.
  - 20 J. Chang, Y. Xiao, M. Xiao, J. Ge, C. Liu and W. Xing, Surface oxidized cobalt-phosphide nanorods as an advanced oxygen evolution catalyst in alkaline solution, *ACS Catal.*, 2015, **5**, 6874.
  - 21 L. A. Stern, L. Feng, F. Song and X. Hu, Ni<sub>2</sub>P as a Janus catalyst for water splitting: the oxygen evolution activity of Ni<sub>2</sub>P nanoparticles, *Energy Environ. Sci.*, 2015, **8**, 2347.
  - 22 J. Sun, M. Ren, L. Yu, Z. Yang, L. Xie, F. Tian, Y. Yu, Z. Ren, S. Chen and H. Zhou, Highly efficient hydrogen evolution from a mesoporous hybrid of nickel phosphide nanoparticles anchored on cobalt phosphosulfide/phosphide nanosheet arrays, *Small*, 2019, **15**, 1804272.
  - 23 F. Yu, H. Zhou, Y. Huang, J. Sun, F. Qin, J. Bao, W. A. Goddard III, S. Chen and Z. Ren, High-performance bifunctional porous non-noble metal phosphide catalyst for overall water splitting, *Nat. Commun.*, 2018, **9**, 2551.
  - 24 A. Mendoza-Garcia, H. Zhu, Y. Yu, Q. Li, L. Zhou, D. Su, M. J. Kramer and S. Sun, Controlled anisotropic growth of Co-Fe-P from Co-Fe-O nanoparticles, *Angew. Chem., Int. Ed.*, 2015, **54**, 9642.
  - 25 J. Xu, H. Zhang, P. Xu, R. Wang, Y. Tong, Q. Lu and F. Gao, *In situ* construction of hierarchical Co/MnO@graphite carbon composites for highly supercapacitive and OER electrocatalytic performances, *Nanoscale*, 2018, **10**, 13702.
  - 26 D. Yang, W. Hou, Y. Lu, W. Zhang and Y. Chen, Scalable synthesis of self-assembled bimetallic phosphide/N-doped graphene nanoflakes as an efficient electrocatalyst for overall water splitting, *Nanoscale*, 2019, **11**, 12837.
  - 27 Y. Hou, Y. Liu, R. Gao, Q. Li, H. Guo, A. Goswami, R. Zboril, M. B. Gawande and X. Zou, Ag@Co<sub>x</sub>P core-shell heterogeneous nanoparticles as efficient oxygen evolution reaction catalysts, *ACS Catal.*, 2017, **7**, 7038.
  - 28 D. Li, H. Baydoun, C. N. Verani and S. L. Brock, Efficient water oxidation using CoMnP nanoparticles, *J. Am. Chem. Soc.*, 2016, **138**, 4006.
  - 29 H. Liao, Y. Sun, C. Dai, Y. Du, S. Xi, F. Liu, L. Yu, Z. Yang, Y. Hou, A. C. Fisher, S. Li and Z. J. Xu, An electron deficiency strategy for enhancing hydrogen evolution on CoP nano-electrocatalysts, *Nano Energy*, 2018, **50**, 273.
  - 30 M. Görlin, J. F. de Araújo, H. Schmies, D. Bernsmeier, S. Dresch, M. Gliech, Z. Jusys, P. Chernev, R. Kraehnert, H. Dau and P. Strasser, Tracking catalyst redox states and reaction dynamics in Ni-Fe oxyhydroxide oxygen evolution reaction electrocatalysts: the role of catalyst support and electrolyte pH, *J. Am. Chem. Soc.*, 2017, **139**, 2070.
  - 31 S. Klaus, L. Trotochaud, M.-J. Cheng, M. Head-Gordon and A. T. Bell, Experimental and computational evidence of highly active Fe impurity sites on the surface of oxidized Au for the electrocatalytic oxidation of water in basic media, *ChemElectroChem*, 2016, **3**, 66.
  - 32 B. S. Yeo and A. T. Bell, Enhanced activity of gold-supported cobalt oxide for the electrochemical evolution of oxygen, *J. Am. Chem. Soc.*, 2011, **133**, 5587.
  - 33 A. L. Strickler, M. Escudero-Escribano and T. F. Jaramillo, Core-shell Au@metal-oxide nanoparticle electrocatalysts for enhanced oxygen evolution, *Nano Lett.*, 2017, **17**, 6040.
  - 34 Y. Xu, S. Duan, H. Li, M. Yang, S. Wang, X. Wang and R. Wang, Au/Ni<sub>12</sub>P<sub>5</sub> core/shell single-crystal nanoparticles as oxygen evolution reaction catalyst, *Nano Res.*, 2017, **10**, 3103.
  - 35 S. Duan and R. Wang, Au/Ni<sub>12</sub>P<sub>5</sub> core/shell nanocrystals from bimetallic heterostructures: *in situ* synthesis, evolution and supercapacitor properties, *NPG Asia Mater.*, 2014, **6**, e00.
  - 36 P. E. R. Blanchard, A. P. Grosvenor, R. G. Cavell and A. Mar, X-ray photoelectron and absorption spectroscopy of metal-rich phosphides M<sub>2</sub>P and M<sub>3</sub>P (M=Cr-Ni), *Chem. Mater.*, 2008, **20**, 7081.
  - 37 A. P. Grosvenor, S. D. Wik, R. G. Cavell and A. Mar, Examination of the bonding in binary transition-metal





- monophosphides MP (M=Cr, Mn, Fe, Co) by X-ray photoelectron spectroscopy, *Inorg. Chem.*, 2005, **44**, 8988.
- 38 A. Dutta, A. K. Samantara, S. K. Dutta, B. K. Jena and N. Pradhan, Surface-oxidized dicobalt phosphide nanoneedles as a nonprecious, durable, and efficient OER catalyst, *ACS Energy Lett.*, 2016, **1**, 169.
- 39 R. Wu, Y. Dong, P. Jiang, G. Wang, Y. Chen and X. Wu, Electrodeposited synthesis of self-supported Ni-P cathode for efficient electrocatalytic hydrogen generation, *Prog. Nat. Sci.: Mater. Int.*, 2016, **26**, 303.
- 40 M. C. Biesinger, B. P. Payne, A. P. Grosvenor, L. W. M. Lau, A. R. Gerson and R. S. C. Smart, Resolving surface chemical states in XPS analysis of first row transition metals, oxides and hydroxides: Cr, Mn, Fe, Co and Ni, *Appl. Surf. Sci.*, 2011, **257**, 2717.
- 41 Y.-J. Yuan, Z.-K. Shen, S. Song, J. Guan, L. Bao, L. Pei, Y. Su, S. Wu, W. Bai, Z.-T. Yu, Z. Ji and Z. Zou, Co-P bonds as atomic-level charge transfer channel to boost photocatalytic H<sub>2</sub> production of Co<sub>2</sub>P/black phosphorus nanosheets photocatalyst, *ACS Catal.*, 2019, **9**, 7801.
- 42 Z. Jin, P. Lia and D. Xiao, Metallic Co<sub>2</sub>P ultrathin nanowires distinguished from CoP as robust electrocatalysts for overall water-splitting, *Green Chem.*, 2016, **18**, 1459.
- 43 L. Yu, Q. Zhu, S. Song, B. McElhenny, D. Wang, C. Wu, Z. Qin, J. Bao, Y. Yu, S. Chen and Z. Ren, Non-noble metal-nitride based electrocatalysts for high-performance alkaline seawater electrolysis, *Nat. Commun.*, 2019, **10**, 5106.

